Characterization of an Integral Protein of the Brush Border Membrane Mediating the Transport of Divalent Metal Ions

Martin Knöpfel,*† Georg Schulthess,‡ Felix Funk,† and Helmut Hauser*

*Institute of Biochemistry, Swiss Federal Institute of Technology, ETH Centre, CH-8092 Zurich; †Institute of Terrestrial Ecology, Swiss Federal Institute of Technology Zurich, CH-8952 Schlieren; and ‡Department of Internal Medicine, Medizinische Poliklinik, University Hospital, CH-8091 Zurich, Switzerland

ABSTRACT The transport of Fe^{2+} and other divalent transition metal ions across the intestinal brush border membrane (BBM) was investigated using brush border membrane vesicles (BBMVs) as a model. This transport is an energy-independent, protein-mediated process. The divalent metal ion transporter of the BBM is a spanning protein, very likely a protein channel, that senses the phase transition of the BBM, as indicated by a break in the Arrhenius plot. The transporter has a broad substrate range that includes Mn^{2+}, Fe^{2+}, Co^{2+}, Ni^{2+}, Cu^{2+}, and Zn^{2+}. Under physiological conditions the transport of divalent metal ions is proton-coupled, leading to the acidification of the internal cavity of BBMVs. The divalent metal ion transporter can be solubilized in excess detergent (30 mM diheptanoylphosphatidylcholine or 1% Triton X-100) and reconstituted into an artificial membrane system by detergent removal. The reconstituted membrane system showed metal ion transport characteristics similar to those of the original BBMVs. The properties of the protein described here closely resemble those of the proton-coupled divalent cation transporter (DCT1, Nramp2) described by Gunshin et al. (1997, *Nature.* 388:482–488). We may conclude that a protein of the Nramp family is present in the BBM, facilitating the transport of Fe^{2+} and other divalent transition metal ions.

INTRODUCTION

Metal ions are cofactors of a variety of essential enzymes participating in biologically important processes and reactions such as oxygen transport and delivery, oxidative phosphorylation, or the control of free radicals. The supply of cells with metal ions is therefore crucial. The iron uptake of mammalian cells by transferrin-receptor-mediated endocytosis and the subsequent transport of iron across endosomal membranes are well established (Dautry-Varsat et al., 1983; Smythe and Warren, 1991). This mechanism, however, is not applicable to iron absorption by small-intestinal epithelial cells (enterocytes). A non-receptor-mediated mechanism involving metal ion transporters at the plasma membrane surface has been implicated in this case (De Silva et al., 1996; Qian et al., 1997). Although many parameters affecting small-intestinal iron absorption are well known, the details of the mechanism underlying this process remain elusive (Marx and Aisen, 1981; Huebers et al., 1987; Conrad et al., 1990, 1996; Trowbridge, 1991; Alvarez-Hernandez et al., 1994; Glahn et al., 1996; Gutierrez and Wessling-Resnick, 1996; Wienk et al., 1996; Gutierrez et al., 1998; Umbreit et al., 1998).

The absorption of nonheme iron is assumed to be preceded by the reduction of Fe^{3+} to Fe^{2+} by ferrireductase (Jordan and Kaplan, 1994; Raja et al., 1992) and ascorbate (Han et al., 1995) and to take place mainly in the proximal small intestine, where iron absorption is facilitated by the acidic environment. Recently Hediger and colleagues identified a divalent-cation transporter by expression cloning in oocytes of *Xenopus laevis* and showed that the protein is ubiquitously expressed, most notably in the proximal duodenum (Gunshin et al., 1997). The protein is a member of the "natural-resistance-associated macrophage protein" (Nramp) family (Vidal et al., 1993; Gruenheid et al., 1995; Gunshin et al., 1997; Savigni and Morgan, 1998; Canonne-Hergaux et al., 1999). The mouse macrophage protein Nramp1 confers resistance to several types of infections in mice; however, the host defense mechanism of Nramp1 is unknown. The amino acid sequence of the divalent-cation transporter described by Gunshin et al. (1997) is 73% identical to human Nramp1 and 92% identical to Nramp2. The divalent-cation transporter is very likely the rat isoform of human Nramp2. Based on functional properties of the protein encoded by the mutated Nramp2 gene in anemic mice and rats (Fleming et al., 1997, 1998) and the functional characteristics of the divalent-cation transporter (Gunshin et al., 1997), the proteins of the Nramp family have been postulated to be divalent-cation transporters. They are essential for normal intestinal iron absorption as well as for iron transport out of endosomes participating in the transferrin cycle (Fleming et al., 1998).

Here we study and characterize the transport of iron and other divalent transition metal ions (particularly Ni^{2+}) across the small-intestinal brush border membrane (BBM). As a model of the BBM we use brush border membrane vesicles (BBMVs) routinely prepared from rabbit duodenum and proximal jejunum. Studies of metal ion transport by plasma membrane vesicles such as BBMVs are hampered by the difficulty that the relatively small amount of

Received for publication 22 October 1999 and in final form 21 April 2000.

Address reprint requests to Dr. Helmut Hauser, Swiss Federal Institute of Technology, Institute of Biochemistry, Universitätstrasse 16, ETH Centre, CH-8092 Zurich, Switzerland. Tel.: 41-1-632-3145; Fax: 41-1-632-1298; E-mail: helmut.hauser@bc.biol.ethz.ch.

© 2000 by the Biophysical Society

0006-3495/00/08/874/11 $2.00

metal ion transported across the membrane is often swamped by the excess of metal ions adsorbed and bound to the membrane surface. As a result the error of the measurement is too large to allow a reliable determination of metal ion transport. To circumvent this problem we designed a fluorescence assay based on calcein that is an adaptation of the fluorescence assay introduced by Breuer et al. (1995). Evidence is presented to show that there is a transport protein in the intestinal BBM facilitating the movement of Fe^{2+} and other divalent transition metal ions across this membrane.

MATERIALS AND METHODS

Materials

Calcein disodium salt, EDTA (ethylenediaminetetraacetic acid disodium salt dihydrate), nitrilotriacetic acid (NTA), $FeCl_2 \cdot 4H_2O$, $FeCl_3 \cdot 6H_2O$, $NiCl_2 \cdot 6H_2O$, and $CuCl_2$ were purchased from Fluka (Buchs, Switzerland); pyranine (trisodium salt of 8-hydroxy-1,3,6-pyrene trisulfonate), laser grade, was from Arcos Organics (Geel, Belgium); $CoCl_2 \cdot 6H_2O$, $MnCl_2 \cdot 4H_2O$, $ZnCl_2$, and $CrCl_3 \cdot 6H_2O$ (all transition metal chlorides were of puriss standard) were from E. Merck (Darmstadt, Germany); egg phosphatidylcholine and egg phosphatidic acid were from Lipid Products (South Nutfield, Surrey, UK); Triton X-100, 4-(2-aminoethyl)-benzenesulfonyl fluoride hydrochloride (AEBSF), and papain from latex of *Carica papaya* as a suspension of crystals in 50 mM sodium acetate buffer (pH 4.5) were from Boehringer (Mannheim, Germany); D,L-dithiothreitol (DTT) and *trans*-epoxysuccinyl-L-leucylamido-(4-guanidino)-butane (E-64) were from Sigma (Buchs, Switzerland); and Sepharose CL-4B was from Pharmacia (Uppsala, Sweden).

Methods

BBMVs were prepared routinely from ~1 m proximal rabbit small intestine comprising duodenum and upper jejunum by the method of Hauser et al. (1980). Small intestines were either frozen and stored at −80°C or freshly excised before the preparation of BBMVs. The resulting BBMVs were characterized according to established methods (Hauser et al., 1980; Schulthess et al., 1996). BBMVs were digested with papain as described previously (Thurnhofer and Hauser, 1990).

Loading of BBMVs and unilamellar phospholipid vesicles with calcein and pyranine

The fluorescent dye calcein was entrapped in the cavity of BBMVs by homogenization of a 0.15-ml suspension of BBMVs (15–20 mg protein/ml) in HEPES buffer (0.05 M HEPES, pH 7.4, 0.1 M NaCl) containing the desired concentration of calcein with a 1 ml Potter-Elvehjem homogenizer at room temperature. The motor-driven pestle of the homogenizer was moved up and down through the BBMV suspension three to five times at 1000 rpm. External calcein was separated from the calcein-loaded vesicles by gel filtration of the BBMV suspension (0.15 ml) on Sepharose CL-4B (1.5 ml packed in a 2-ml graduated pipette) equilibrated and run with HEPES buffer. The calcein concentration entrapped in the BBMV cavity was usually 30 or 33 μM; concentrations greater than 37 μM were not used because of self-quenching of calcein. The average size and size distribution of BBMVs and calcein-loaded BBMVs were determined routinely by freeze-fracture electron microscopy (Hauser et al., 1983; Perevucnik et al., 1985). The amount of calcein bound to the outer membrane surface of BBMVs was determined by incubating BBMVs with calcein at room temperature for approximately the same period of time used to homogenize BBMVs. Unbound calcein was removed by gel filtration as described above, and the fluorescence intensity of the BBMVs containing bound calcein was determined and converted to calcein concentration by means of an appropriate calibration curve. The pH-sensitive fluorescent dye pyranine was entrapped in BBMVs as described for calcein, except that the pyranine concentration was 0.5 mM.

Calcein-loaded small unilamellar vesicles (SUVs) consisting of egg phosphatidylcholine (PC) were produced by tip sonication (Branson sonifier, model B30, with a standard microtip) of the phospholipid dispersion in HEPES buffer containing 30 μM calcein. Calcein-loaded large unilamellar vesicles (LUVs) consisting of egg PC/egg phosphatidic acid (PA) (mole ratio = 1:1) were made by dispersing the dried lipid film in HEPES buffer containing 30 μM calcein. The calcein was entrapped in reconstituted BBMVs in the same way as described for BBMVs. In all cases external calcein was separated from entrapped calcein by gel filtration on Sepharose CL-4B as described above for the production of calcein-loaded BBMVs.

Measurement of transport of iron and other transition metal ions into BBMVs, using two continuous fluorescence assays

Two continuous fluorescence assays based on calcein were used to measure the transport of Fe^{2+} and other divalent transition metal ions to and across the BBM into the cavities of these vesicles. Both assays are based on the fact that calcein is membrane-impermeable and the calcein fluorescence is quenched as a result of the formation of metal ion-calcein complexes. In assay A, BBMVs are added at time 0 to a calcein solution (30 or 33 μM) quenched by an excess of divalent transition metal ions. Upon the addition of BBMVs, metal ions interact with the external surface of the BBM, and some ions are transported across the BBM into the vesicle cavity. As a result, the quenching of the membrane-impermeable calcein is released as indicated by a concomitant increase in fluorescence intensity.

In assay B transition metal ions are added to calcein-loaded BBMVs at time 0. In this case metal ions crossing the membrane and entering the vesicle cavity elicit quenching of calcein, as indicated by a decrease in fluorescence intensity. However, only those metal ions transported into the vesicle cavity that remain in solution, in equilibrium with metal ions bound to the inner membrane surface, contribute to quenching. With method B there is a complication at temperatures above 25°C. We observed that the metal ion transport into the vesicle cavity at temperatures higher than ~25°C is coupled to proton cotransport, leading to the acidification of the vesicle cavity and concomitant quenching of calcein. With proton cotransport taking place we were unable to discern the contribution to quenching due to metal ion-calcein complex formation and acidification of the vesicle cavity. In this case we refrained from converting fluorescence intensity changes to metal ion concentrations. Therefore kinetic curves measured at temperatures above ~25°C are presented as fluorescence intensity in arbitrary units as a function of time.

Calcein fluorescence intensities (excitation 490 nm, emission 514 nm) and pyranine fluorescence intensities (excitation 455 nm, emission 512 nm) were measured in a Spex Fluorolog Double Spectrometer (from Spex Industrials S. A. Group, Edison, NJ) attached to a Compaq Deskpro XE560 Computer with a Spex Spectracq interface at room temperature unless stated otherwise. For each calcein concentration and transition metal ion used in assays A and B, a quenching curve was constructed that related fluorescence intensity to the total metal ion concentration. These experimental quenching curves were fitted adequately by an exponential function:

$$I = \frac{1}{w\sqrt{\pi}} \exp\left[-\left(\frac{x - x_o}{w} \right)^2 \right] \quad (1)$$

where I is the fluorescence intensity, w and x_o are constants, and x is the transition metal ion concentration. Equation 1 was used to convert fluorescence intensities I to metal ion concentrations present in the calcein-containing compartment, which is the external medium of BBMVs (assay

A) or the internal cavity of BBMVs (assay B). Assay A therefore determines the metal ion concentration in the external medium of BBMVs. Knowing the total metal ion concentration added, we obtain the concentration (amount) of metal ions that interacts with BBMVs by subtraction of the metal ion concentration determined by assay A from the total metal ion concentration. The amount of metal ions interacting with BBMVs consists of two contributions, 1) metal ions bound and adsorbed to the external membrane surface and 2) metal ions transported into the vesicle cavity. The latter contribution consists of metal ions bound to the inner membrane surface and free metal ions present in the vesicle cavity. An estimate of the free metal ion concentration in the BBMV cavity is obtained with assay B.

Special precautions were taken for Fe^{2+} transport measurements. Fe^{2+} solutions were made in HEPES buffer gassed with N_2, and all manipulations of the samples were carried out under N_2 with a glove box. Before transport measurements in the Spex fluorimeter the samples were flushed with Ar.

Kinetic curves of metal ion transport were fitted by a single exponential or the sum of exponentials:

$$y = 1 - [y_\infty + A \exp(-k_1 t)] \quad (2)$$

$$y = 1 - \left[y_\infty + \sum_{n=1}^{n} A_n \exp(-k_n t) \right] \quad (3)$$

where y_∞ is the y value at equilibrium, A_n is the amplitude of phase n, and k_n is the corresponding pseudo-first-order rate constant. Half-times $t_{1/2}$ were calculated from k_n as

$$t_{1/2} = \ln 2/k_n \quad (4)$$

For curve fitting the programs Origin 4.1 (Microcal Software), MacCurveFit (Kevin Raner Software, Victoria, Australia), and Excel (Microsoft) were used on a Macintosh Computer.

Reconstitution of the metal ion transport activity

The solubilization of BBMVs in 30 mM diheptanoyl PC and the reconstitution of the solubilized BBM protein(s) responsible for the transport of Fe^{2+} and other transition metal ions was carried out according to published methods (Boffelli et al., 1997). Alternatively, BBMVs were solubilized with Triton X-100. A freshly thawed dispersion of BBMVs (~20 mg protein/ml) was diluted 20-fold with HEPES buffer, and BBMVs were pelleted at 45,000 × *g* for 20 min at 4°C. The supernatant was decanted, and the pellet of BBMVs was solubilized in HEPES buffer containing 1% Triton X-100, 1 mM AEBSF, and 10 μM E-64. The resulting dispersion was centrifuged at 130,000 × *g* for 10 min at 4°C, and the supernatant was carefully collected. For reconstitution 1 ml of the supernatant containing 1 mg protein was added to a dried lipid film of 10 mg egg PC and egg PA (mole ratio 1:1) at room temperature, the lipid film was dispersed by vortexing, and the reconstitution was initiated by dropwise dilution of the dispersion by 300-fold with HEPES buffer to a final Triton X-100 concentration of 0.05 mM. This is below the critical micellar concentration of Triton X-100, given as 0.2 mM at 25°C in the supplier's catalog. The reconstituted membrane vesicles were pelleted by centrifugation at 142,000 × *g* for 90 min at 4°C and resuspended in HEPES buffer. The resulting vesicles were washed twice by centrifugation and resuspension in HEPES buffer.

Analytical methods

Phospholipid concentrations were determined as described before (Hauser et al., 1980), and protein concentrations were determined by the bicinchoninic acid method of Pierce Chemical Co. (Boffelli et al., 1997). Sodium dodecyl sulfate-polyacrylamide gel electrophoresis (SDS-PAGE) was carried out in a Mini-Protean II dual slab cell from Bio-Rad according to the Bio-Rad instruction manual. Protein standards from Bio-Rad were used as molecular weight markers. Proteins were visualized by Coomassie blue staining.

RESULTS

Characterization of BBMVs and calcein-loaded BBMVs

The size and size distribution of empty BBMVs and BBMVs containing calcein in their cavities were identical within experimental error, as determined by freeze-fracture electron microscopy. The average diameters were 163 ± 59 nm (n = 124) and 160 ± 64 nm (n = 37), respectively, in good agreement with published data (Perevucnik et al., 1985). The volume of the internal cavities of BBMVs determined from the fluorescence intensity of entrapped calcein was V_{in} = 1.9 ± 0.2 μl/mg protein. This value was corrected for calcein bound to the outer membrane surface of BBMVs, which amounted to 20–25% of the total calcein associated with loaded BBMVs. Assuming that a similar amount of calcein is bound to the inner surface of BBMVs, the value for the internal volume of BBMVs reduces to 1.5 μl/mg, a value in good agreement with published data (Semenza et al., 1984; Perewusnyk and Funk, 1997).

That calcein was indeed entrapped in the cavity of BBMVs was shown by gel filtration on Sepharose CL-4B of calcein-loaded BBMVs in the absence and presence of Triton X-100. In the absence of detergent, calcein-loaded BBMVs were eluted in the column void volume; the protein peak of BBMVs coincided with the calcein peak. In contrast, in the presence of 1% Triton X-100 most of the calcein was eluted in the total column volume, well separated from the protein peak eluted in the void volume (data not shown).

When calcein-loaded BBMVs suspended in HEPES buffer were exhaustively dialyzed against the same buffer at 4°C for ~1 day, ~12% of the total calcein associated with BBMVs was lost into the dialysate, indicating that calcein-loaded BBMVs are stable at 4°C for hours. In contrast, pelleting of calcein-loaded BBMVs by centrifugation at 15,800 × *g* for 15 min at 4°C caused leakage of calcein. Centrifugation under these conditions reproducibly released 50% of the entrapped calcein. Rehomogenization of calcein-loaded BBMVs under the conditions described for the loading of BBMVs with calcein (see Methods) had the same effect as centrifugation: ~50% of the entrapped calcein was released. These experiments clearly show that calcein-loaded BBMVs break up during centrifugation and pelleting, partially releasing their content.

Kinetics of transition metal ion transport across the BBM

The calcein fluorescence assays (assays A and B) allowed us to determine 1) the total amount of metal ions that

equilibrate with BBMVs and 2) the amount of metal ions that are transported across the BBM, and to measure 3) the kinetics of metal ion binding to the outer surface of BBMV and 4) the kinetics of metal ion transport across the BBM. For each calcein concentration and for each transition metal ion used in either assay A or assay B a calibration curve was constructed that relates fluorescence intensity I to the total metal ion concentration (Fig. 1). These calibration curves were fitted by Eq. 1 and used to convert fluorescence intensities I to metal ion concentrations present in the calcein-containing compartment, that is, the external medium in assay A and the internal cavities of BBMVs in assay B.

Representative kinetic curves of Ni^{2+} transport to and into BBMVs obtained with fluorescence assay A are shown in Fig. 2 *A*. Satisfactory fits to these curves were obtained by using the sum of three exponential functions (cf. Eq. 3). The initial phase was too fast to be resolved on the time scale of this experiment. An upper limit of the half-time of 20 s ($n = 13$) was derived for this process, which is thought to represent the interaction of Ni^{2+} with the external membrane surface of BBMVs. The average value of the pseudo-first-order rate constant of the second slower process assigned to the transport of metal ions across the BBM was $k_1 = 0.34 \pm 0.1\ min^{-1}$ ($t_{1/2} = 2.0$ min; $n = 11$). This value was found to be independent of the BBMV concentration over the range of 0.22–3.5 mg protein/ml. The third phase was characterized by a pseudo-first-order rate constant $k_1 = 0.026 \pm 0.001\ min^{-1}$ ($t_{1/2} = 27$ min; $n = 15$), the origin of which is unknown. As the total Ni^{2+} concentration was raised in the external medium the amount of Ni^{2+} bound to BBMVs after incubation for 30 min increased progressively (Fig. 2 *A*) and linearly with the total Ni^{2+} concentration (data not shown). From the slope of the straight line obtained by plotting $[Ni^{2+}]_b$ versus total $[Ni^{2+}]$, the amount of Ni^{2+} bound to BBMVs was derived as 40 ± 1% of the total Ni^{2+} concentration. This result is consistent with the notion that Ni^{2+} detected by assay A is equilibrated with the BBM surfaces and the internal cavity of BBMV. Application of the mass action law supports this conclusion:

$$K_d = \frac{[Ni^{2+}]_f[BBMV]_f}{[Ni^{2+}]_b} \quad (5)$$

where $[Ni^{2+}]_f$ and $[Ni^{2+}]_b$ are the free and bound Ni^{2+} concentrations, respectively; $[BBMV]_f$ is the concentration of free chelating groups at the BBM surface; and K_d is the dissociation constant. If we assume that $[BBMV]_f$ is present in large excess relative to the total Ni^{2+} concentrations used in Fig. 2 *A*, Eq. 5 reduces to $[Ni^{2+}]_f/[Ni^{2+}]_b = K_d'$. Using this expression, we obtained an average K_d' value of 1.51 ± 0.01 for the five Ni^{2+} concentrations used in Fig. 2 *A*. This result is good evidence that the plateau concentrations of Ni^{2+} transport shown in Fig. 2 *A* are indeed equilibrium concentrations.

In Fig. 2 *B* kinetic curves are presented for transport of Ni^{2+} into the cavities of BBMVs, as determined by assay B. These curves were fitted adequately by the sum of two exponential functions. Similar to the results obtained with the fluorescence assay A, the first phase was too fast to be resolved on the time resolution of our experiment. An estimate derived for the upper limit of the half-time of this process was 10 s and was of the same order as the half-time of the initial fast phase detected by assay A. The first phase is therefore interpreted to represent the interaction of Ni^{2+} with calcein bound to the external surface of BBMVs. This assignment is supported by the following observation: the amplitude A (see Eq. 3) of the first phase derived from curve fitting was 20 ± 5%, in good agreement with the amount of calcein bound to the outer surface of BBMVs. The pseudo-first-order rate constant derived for the second slow phase was $k_1 = 0.3 \pm 0.1\ min^{-1}$ ($t_{1/2} = 2.4$ min; $n = 4$). These values are in good agreement with the kinetic parameters derived from the second slower phase of Ni^{2+} transport measured with assay A (Fig. 2 *A*). The second slower phase (Fig. 2 *B*) was therefore assigned to Ni^{2+} transport across the BBM into the cavity of these vesicles. We note from a comparison of Fig. 2, *A* and *B*, that the amount of Ni^{2+} detected by assay B is ~1/1000 of that detected by assay A. Furthermore, the quantities of Ni^{2+} transported to and into the BBMVs at equilibrium (Fig. 2 *B*) were linearly related to the total Ni^{2+} concentration (data not shown). A simple calculation showed that the Ni^{2+} concentrations present in the vesicle cavity at equilibrium approximate the external Ni^{2+} concentration, supporting the notion that Ni^{2+} ions equilibrate with BBMVs.

Fig. 3 *A* shows the kinetics of Ni^{2+} transport into BBMVs at 6°C, 12°C, 24°C, and 37°C, as detected by assay B. As mentioned for Fig. 2 *B*, these curves were adequately fitted by a double-exponential function from which pseudo-first-order rate constants k_1 were derived. The k_1 values derived

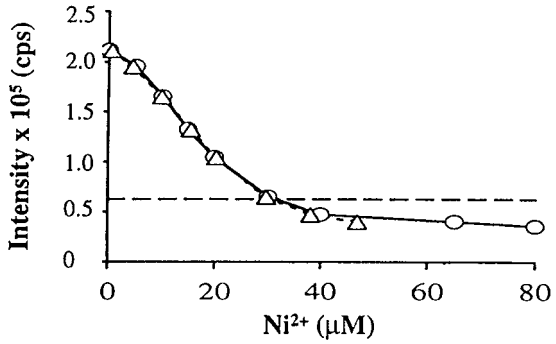

FIGURE 1 A typical quenching curve is shown for a 33 μM calcein solution in HEPES buffer in the presence of increasing concentrations of Ni^{2+}. The experimental curve (○) relating fluorescence intensity I in cps to the total Ni^{2+} concentration was fitted by Eq. 1 (△), and from the curve fit the Ni^{2+} concentration in the external medium (assay A) or the internal vesicle cavity (assay B) was derived. In both assays A and B the branch of the calibration curve above the dashed line was used to convert intensities into Ni^{2+} concentrations.

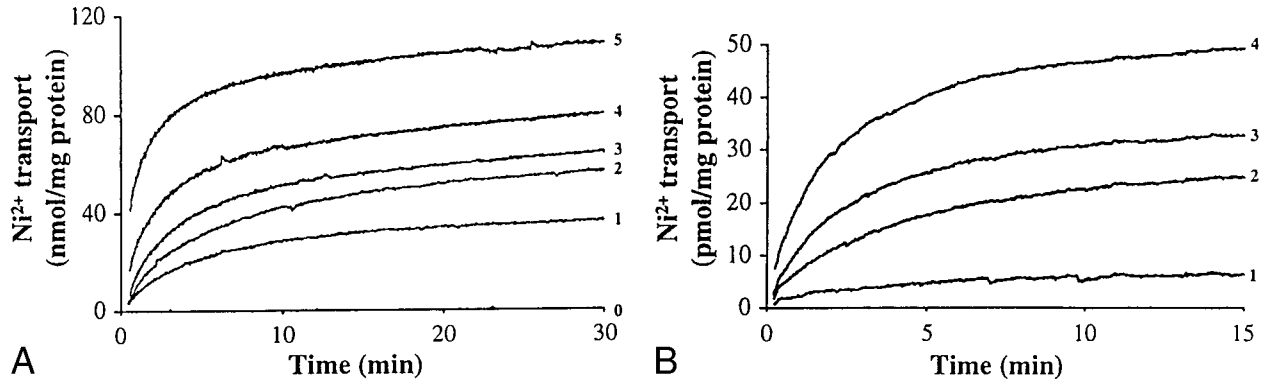

FIGURE 2 (*A*) Kinetic curves obtained with assay A for the interaction of Ni^{2+} with BBM at 22°C. At time 0 BBMVs (0.6 mg protein/ml) were added to a solution of 30 μM calcein and different Ni^{2+} concentrations. Changes in fluorescence intensity were recorded as a function of time for Ni^{2+} concentrations of 0 μM (*0*), 71 μM (*1*), 88 μM (*2*), 106 μM (*3*), 132 μM (*4*), and 176 μM (*5*) (*bottom to top*). The increase in fluorescence intensities was converted to Ni^{2+} (nmol/mg protein) transported to and into BBMVs. (*B*) Kinetic curves obtained with assay B for the transport of Ni^{2+} across the BBM at 22°C. At time 0 calcein-loaded BBMVs (0.4 mg protein/ml with an internal calcein concentration of 31 μM) were mixed with Ni^{2+} concentrations of 19 μM (*1*), 38 μM (*2*), 63 μM (*3*), and 94 μM (*4*) (*bottom to top*).

from curve fitting for the second slower phase were temperature dependent (Table 1). Plotting these k_1 values as an Arrhenius plot reproducibly yielded three straight lines with points of intersection at 5 ± 1°C and 24 ± 1°C (Fig. 3 *B*). From the slopes of these straight line relations activation energies E_a were derived: below 5°C E_a = 153.0 kJ/mol (36.6 kcal/mol), between 5°C and 24°C E_a = 21.2 kJ/mol (5.09 kcal/mol), and above 24°C E_a = 62.0 kJ/mol (14.8 kcal/mol).

The kinetics of Ni^{2+} and Fe(III) transport into BBMVs at room temperature, determined by fluorescence assay A, are compared in Fig. 4. The relatively fast and efficient transport of Ni^{2+} is in contrast to the limited transport of Fe(III) administered as the NTA complex (mole ratio 1:2). The values obtained for the transport over 20 min were 105.0 ± 0.8 nmol/mg protein for Ni^{2+} and 5 ± 4 nmol/mg protein for Fe (III), in good agreement with published data (Perewusnyk and Funk, 1997).

The kinetics of Fe^{2+} transport into the cavity of BBMVs at 18°C and 37°C determined by assay B are compared in Fig. 5 *A*. At the two temperatures, similar equilibrium values for Fe^{2+} were obtained; however, at 37°C an appar-

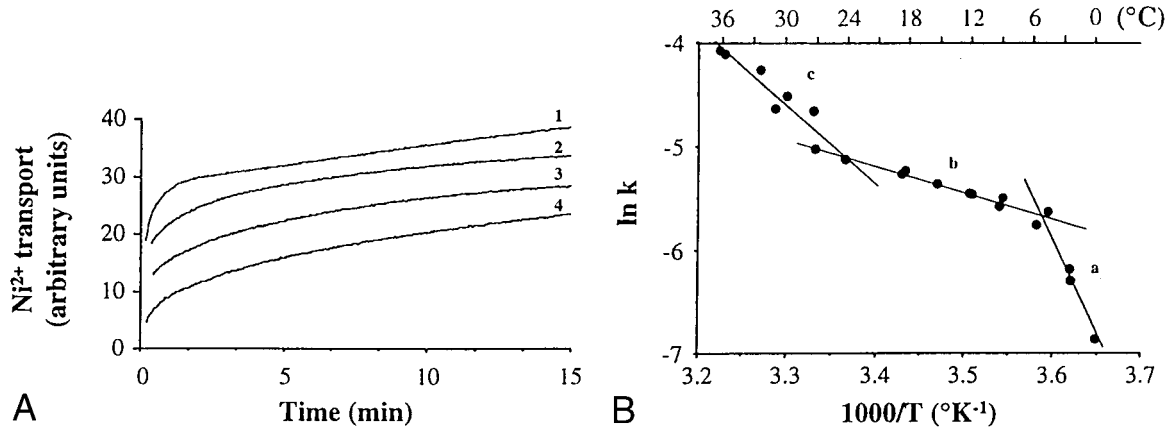

FIGURE 3 (*A*) Kinetics of Ni^{2+} transport across the membrane of BBMVs measured at different temperatures. Calcein-loaded BBMVs (0.9 mg protein/ml with an internal calcein concentration of 33 μM) were mixed at time 0 with Ni^{2+} ([Ni^{2+}] = 0.1 mM), and kinetic curves were recorded at 6°C (*4*), 12°C (*3*), 24°C (*2*), and 37°C (*1*) (*bottom to top*), using the fluorescence assay B. (*B*) Arrhenius plot of ln k_1 as a function of 1/*T*. Pseudo-first-order rate constants k_1 were derived from curve fitting of the kinetic curves similar to those shown in *A*. The data points of the Arrhenius plot were best fitted by three straight lines intersecting at 5 ± 1°C and 24 ± 1°C. Below 5°C the straight line *a* is given by $y = 60.3 - 18{,}400x$ ($R^2 = 0.911$), yielding an energy of activation of E_a = 153 kJ/mol (36.6 kcal/mol); above 5°C the straight line *b* is given by $y = 3.52 - 2561x$ ($R^2 = 0.957$), yielding an activation energy of E_a = 21.2 kJ/mol (5.09 kcal/mol); and at temperatures above 24°C the straight line *c* is given by $y = 20.0 - 7463x$ ($R^2 = 0.907$; E_a = 62.0 kJ/mol = 14.8 kcal/mol). Apparent energies of activation E_a for Ni^{2+} transport across the BBM were obtained from the slopes of the straight lines: slope = $-E_a/R$, where R is the gas constant.

TABLE 1 Temperature dependence of pseudo-first-order rate constants k_1 for Ni^{2+} transport across the brush border membrane

Temperature (°C)	k_1 (min^{-1})	half-time $t_{1/2}$ (min)
3	0.11 ± 0.02	6.3
6	0.19 ± 0.03	3.6
12	0.26 ± 0.01	2.7
18	0.32 ± 0.02	2.2
24	0.36 ± 0.03	1.9
31	0.59 ± 0.03	1.2
37	1.7 ± 0.1	0.40

ent overshoot of Fe^{2+} transport was observed. A likely explanation of the apparent overshoot is provided by the results depicted in Fig. 5 *B*. The transport of Zn^{2+} into the cavities of BBMVs was measured at 37°C under conditions otherwise comparable to those of Fig. 5 *A*. In contrast to other transition metal ions such as Ni^{2+} and Fe^{2+}, Zn^{2+} has no quenching capacity. Nevertheless, when Zn^{2+} was added to calcein-loaded BBMVs, changes in fluorescence intensity were observed that corresponded to an apparent overshoot (Fig. 5 *B*). Because the overshoot observed in this case cannot be due to quenching by Zn^{2+} and because the fluorescence of calcein is pH dependent (Fig. 5 *C*), we propose that the overshoot is the result of acidification of the vesicle cavity due to proton cotransport with the metal ion. For Zn^{2+} transport the calibration curve (Fig. 5 *C*) was used to convert fluorescence intensity to $[H^+]$ or pH.

Independent, direct evidence for the cotransport of divalent transition metal ions and protons was provided by transport measurements using BBMVs containing the pH-sensitive fluorochrome pyranine in their cavity. Measuring the transport of Mn^{2+}, Co^{2+}, and Zn^{2+} (all at 80 μM) into pyranine-loaded BBMVs at 37°C, we observed a transient overshoot similar to that observed with calcein-loaded BBMVs. Using a calibration curve relating pyranine fluorescence intensity to pH, we converted the overshoot to

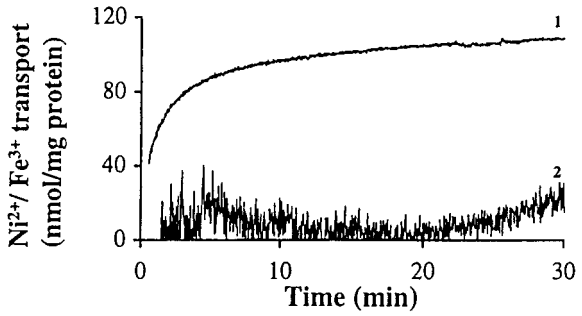

FIGURE 4 Kinetic curves obtained with assay A for Ni^{2+} and Fe^{3+} transport into BBMVs at 22°C. At time 0 BBMVs (0.6 mg protein/ml) were added to a solution of 30 μM calcein and 175 μM Ni^{2+} (*curve 1*), and for curve 2 BBMVs (0.54 mg protein/ml) were added to a 33 μM calcein solution containing Fe^{3+} ($[Fe^{3+}]$ = 199 μM) as the NTA complex ([NTA] = 400 μM).

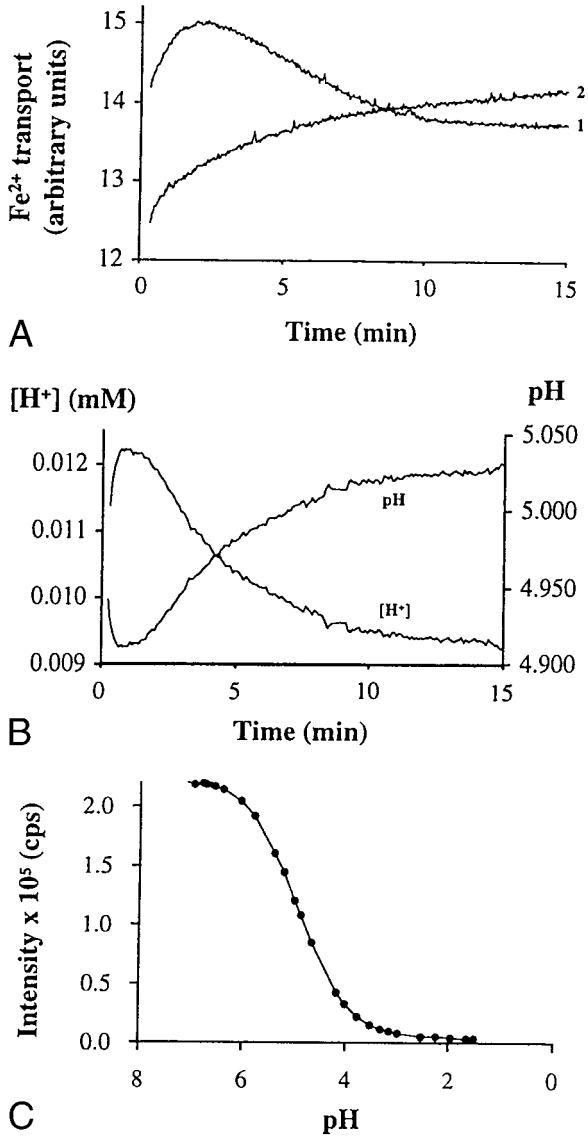

FIGURE 5 (*A*) Kinetics of Fe^{2+} transport across the membrane of BBMVs at 37°C (*curve 1*) and 18°C (*curve 2*), measured with assay B. Calcein-loaded BBMVs (~1 mg protein/ml) containing calcein entrapped in their vesicle cavity ([calcein] = 33 μM) were mixed at time 0 with Fe^{2+} ($[Fe^{2+}]$ = 75 μM). (*B*) Kinetics of Zn^{2+} transport across the membrane of BBMVs at 37°C. Experimental conditions were as in *A*. The transport of Zn^{2+} into the vesicle cavity was detected by changes in the fluorescence intensity of the entrapped calcein due to the acidification of the vesicle cavity, concomitant to metal ion transport. (*C*) The fluorescence intensity of calcein is pH-dependent, and changes in fluorescence intensity were converted to changes in $[H^+]$ or pH, using a calibration curve relating fluorescence intensity to pH. The solid line was obtained by curve fitting, using the Henderson-Hasselbalch equation. The pK value of calcein derived from this fit is 4.9.

$[H^+]$ or the pH of the vesicle cavity. For Zn^{2+} transport the acidification of the cavity was entirely consistent with the data of Fig. 5 *B*. As a control the pyranine fluorescence was shown to be unaffected in the presence of these metal ions.

Fig. 6 illustrates the efficient transport of different transition metal ions across the BBM into the cavity of BBMVs as determined by fluorescence assay B. At 37°C overshooting resulting from the acidification of the vesicle cavity was observed for Cu^{2+}, Co^{2+}, and Mn^{2+}, but not for Ni^{2+}. The kinetic curves of Cu^{2+}, Co^{2+}, and Mn^{2+} transport (Fig. 6) were not sufficiently resolved to allow the determination of rate constants, yet it is clear from the overshoot that the transport of Cu^{2+}, Co^{2+}, and Mn^{2+} is significantly faster than that of Ni^{2+}.

Papain digestion of the BBMVs, which released 60–65% of the membrane protein, had no significant effect on the transport rate of Fe^{2+} and other transition metal ions. Furthermore the temperature dependence of the rate of Ni^{2+} transport in the range from 0°C to 37°C was not significantly changed when we used papain-treated BBMVs (data not shown). This result shows either that the protein responsible for the facilitated metal ion transport is not degraded by papain or the cleavage of extracellular domains of this protein does not disrupt the transport mechanism.

The following control experiments rule out some possible artefacts. It is conceivable that positively charged metal ions interact with the negatively charged lipid bilayer and proteins of the BBM, and as a result the BBM may be perturbed and become leaky to metal ions. This possibility is ruled out based on control experiments summarized in Fig. 7. LUVs of egg PC and egg PA (mole ratio = 1:1) loaded with calcein (33 μM) were incubated without Ni^{2+} and with Ni^{2+} concentrations of 90 μM and 180 μM. As shown in Fig. 7, there was no change in fluorescence intensity with time in the absence (*curve 1*) and in the presence (*curves 2* and *3*) of Ni^{2+}. This is true for periods of time up to 20 min that are typically used in kinetic experiments (data not shown). Calcein-loaded SUVs behaved similarly. These results indicate that the barrier properties of the negatively charged phospholipid bilayer were maintained in the presence of Ni^{2+} up to 180 μM. In contrast, with the addition of 1.2% Triton X-100 the fluorescence intensity decreased in a dose-dependent fashion, indicating that under these conditions the bilayer becomes permeable to metal ions, and as a result the calcein fluorescence is quenched. These results are also consistent with the observation of an overshoot (cf. Figs. 5, 6, 8). The following experiments showed that the integrity of the BBM is maintained in the presence of divalent metal ions at concentrations used in this study. BBMVs were digested with trypsin in the absence of Triton X-100 and in the presence of sufficient Triton X-100 (2%) to solubilize the BBMVs. The reaction products were analyzed by SDS-10% PAGE, and from this analysis it was evident that actin as a protein marker of the inner membrane surface of BBMVs (Semenza et al., 1984) is only digested with trypsin after the solubilization of BBMVs with excess detergent. When BBMVs were digested with trypsin in the presence of 0.1 mM Ni^{2+}, actin was shown to be intact by SDS-PAGE. However, when 2% Triton X-100 was added under these conditions, actin was digested in the same way as in the absence of Ni^{2+} (data not shown).

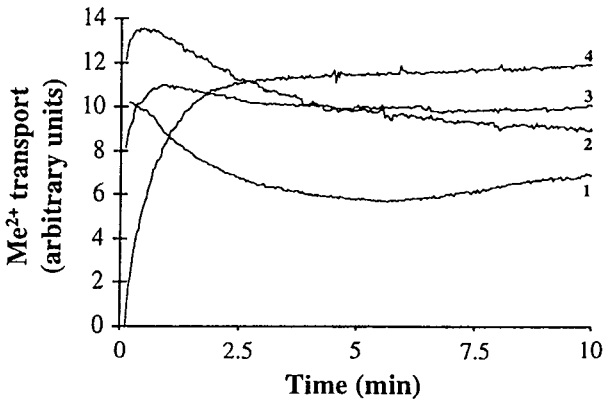

FIGURE 6 Kinetics of the transport of different transition metal ions across the membrane of BBMVs. Calcein-loaded BBMVs (1 mg protein/ml with an entrapped calcein concentration of 33 μM) were mixed at time 0 with Cu^{2+} (*curve 1*, final concentration 80 μM), Mn^{2+} (*curve 2*, 75 μM), Co^{2+} (*curve 3*, 75 μM), and Ni^{2+} (*curve 4,* 75 μM), and the transport of these ions into the vesicle cavity was measured at 37°C with assay B.

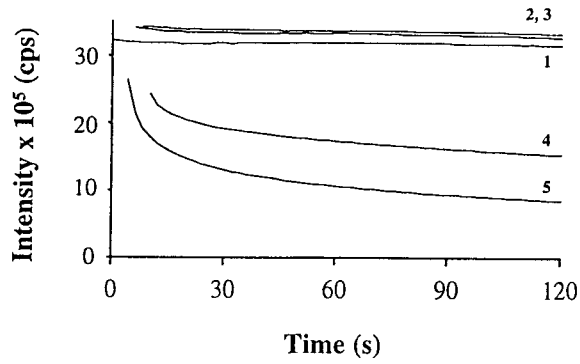

FIGURE 7 Control experiments showing the integrity of negatively charged LUVs made of egg PC/egg PA (mole ratio 1:1) in the presence of Ni^{2+}. Calcein-loaded LUVs were made in HEPES buffer as described in Methods, and at time 0 these LUVs were mixed with buffer (*curve 1*) or Ni^{2+} solutions in buffer to yield final Ni^{2+} concentrations of 90 μM (*curve 2*) and 180 μM (*curve 3*). With the addition of 1.2% Triton X-100 the lipid bilayer of LUV became leaky to Ni^{2+}, and the fluorescence of calcein was quenched in the presence of 80 μM Ni^{2+} (*curve 4*) and 165 μM Ni^{2+} (*curve 5*).

Reconstitution of the divalent metal ion transport protein into an artificial membrane system

BBMVs were solubilized in excess diheptanoyl PC or Triton X-100, yielding mixed lipid-protein micelles. Membrane proteins thus solubilized were reconstituted into an artificial membrane system as described in Methods. Using either isoelectric egg PC or negatively charged phospholipids, e.g., a mixture of egg PC/egg PA (mole ratio = 1:1), we

successfully reconstituted the metal ion transport activity, as demonstrated in Fig. 8. In terms of transport kinetics of Fe^{2+} (Fig. 8) and other divalent metal ions (data not shown), the reconstituted membrane vesicles closely resembled the original BBMVs. Fe^{2+} transport exhibited an apparent overshoot, but with the limited time resolution of the measurement it was not possible to derive a rate constant. However, the equilibrium value of Fe^{2+} transport was increased by a factor of ~10 compared to native BBMVs.

DISCUSSION

Characterization of BBMVs and calcein-loaded BBMVs

A prerequisite of the fluorescence assays used here is that the fluorescent dye can be incorporated into the cavities of BBMVs. Loading of BBMVs with calcein or pyranine is accomplished by homogenization of the BBMVs: this apparently opens the vesicles so that the dye can equilibrate with the vesicle cavity. In loading BBMVs with calcein or pyranine we make good use of the fact that BBMVs break up upon homogenization and reseal right side out (Klip et al., 1979; Haase et al., 1978). As a result any carrier or transport protein maintains its correct vectorial orientation in the membrane.

The following lines of evidence support the notion that calcein-loaded BBMVs are indeed closed and stable in the course of the metal ion transport measurement, i.e., that the membrane integrity is preserved in the course of the transport measurement: 1) Long-term dialysis released not more than ~12% of the calcein. This calcein probably originates from molecules bound to the external surface of the BBM.

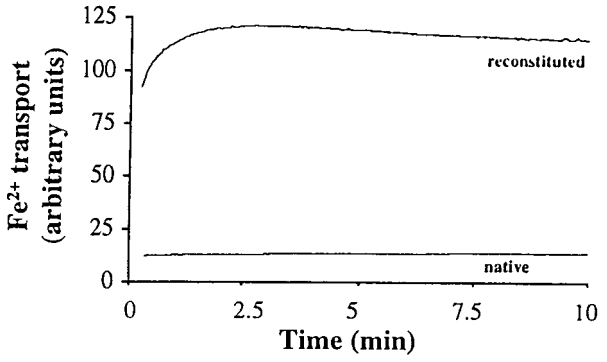

FIGURE 8 Kinetics of Fe^{2+} transport across the membrane of vesicles reconstituted as described in Methods. For reconstitution, BBMVs were solubilized in 1% Triton X-100 and reconstituted to an artificial membrane system as described in Methods. These vesicles were loaded with calcein (final concentration 33 μM) in the same way in which original BBMVs were (see Methods). At time 0 50 μM Fe^{2+} were added to the reconstituted system (0.2 mg membrane protein/ml), and Fe^{2+} transport was measured at 37°C, using the fluorescence assay B. For comparison the Fe^{2+} transport of native BBMVs measured at 37°C is included.

2) Solubilization of BBMVs in excess detergent produced maximum quenching of the entrapped calcein by externally added transition metal ions (Fig. 7). 3) The overshoot or temporary acidification of the cavities of BBMVs due to proton cotransport is incompatible with leaky BBMVs. It is good evidence for the integrity of the BBM in the presence of metal ions up to concentrations of ~100 μM. 4) The controls carried out with BBMVs and negatively charged phospholipid bilayers indicate that the integrity of both structures is maintained in the presence of divalent metal ions at concentrations used in this work. Taking the control experiments together, we can conclude that the integrity of the BBMVs is maintained in the presence of divalent metal ions. An interesting observation that has not been put on record is the instability of BBMVs induced by centrifugation under conditions that pellet the vesicles. This observation is interpreted to indicate that the membrane of BBMVs is transiently disrupted when BBMVs are pelleted, so that the entrapped medium can equilibrate between the membrane surfaces and the total aqueous volume.

Kinetics of transition metal ion transport across the BBM

The pseudo-first-order rate constants k_1 derived from the second slower phase observed with both assays A and B (cf. Fig. 2, *A* and *B*) agree within the error of the measurement and are interpreted to represent the transport of Ni^{2+} across the BBM into the cavity of BBMVs. Both assays are apparently capable of monitoring the kinetics of Ni^{2+} transport across the BBM, despite the fact that most of the Ni^{2+} that interact with BBMVs are bound to the membrane surfaces. This is so because the kinetics of the electrostatic interaction of metal ions with the membrane surface are much faster than the metal ion transport across the membrane, and therefore the former process is clearly discernible from the actual transport of metal ions across the BBM. This is a significant advantage of the continuous fluorescence assays used here, and the combined use of assays A and B appears to be superior to the radiotracer technique.

The kinetics observed in the second, slower phase of metal ion transport, using either assay A or B, are too fast to be explained by passive diffusion across the BBM. With metal ion leakage ruled out, the data presented in Figs. 2–6 and 8 can only be rationalized by postulating a protein-mediated process. Because BBMVs are not energized, this facilitated mechanism must be energy independent. The main conclusion of our study is then that Fe^{2+} is transported across the BBM in an energy-independent, facilitated way.

Searching for metal ions that are not transported in a facilitated way across the BBM, we discovered that the transport of the transition metal ions Mn^{2+}, Co^{2+}, Ni^{2+}, Cu^{2+}, and Zn^{2+} is protein-mediated just as the Fe^{2+} transport is. Using the overshoot measured at 37°C as a kinetic parameter, we obtain an approximate order of the efficiency

of the divalent metal ion transport: $Cu^{2+} > Zn^{2+} > Mn^{2+} > Co^{2+} > Fe^{2+} \gg Ni^{2+}$. Because the ionic radii of the divalent transition metal ions lie within a narrow range, it is unlikely that different proteins are responsible for the metal ion transport. Furthermore, competition experiments using Ni^{2+} in the presence of equal concentrations of another divalent transition metal ion are consistent with a single transport protein (publication in preparation). The competition experiments indicate that the two metal ions compete for the same transport protein. In this context the effect of excess Ca^{2+} was examined because Ca^{2+} was reported to partially inhibit the Fe^{2+} transport in *Xenopus* oocytes (Gunshin et al., 1997). Excess Ca^{2+} up to 10 mM had no inhibitory effect on the transport of divalent transition metal ions into BBMVs. On the contrary, a slight increase in the transport activity was observed. This activation may be a purely electrostatic effect in that divalent transition metal ions bound to the external surface of the BBM are displaced in the presence of excess Ca^{2+} and become available to transport.

The results presented here are therefore consistent with the hypothesis that there is a divalent metal ion transport protein in the BBM capable of transporting a broad range of metal ions, including Mn^{2+}, Fe^{2+}, Co^{2+}, Ni^{2+}, Cu^{2+}, and Zn^{2+}. The rather limited availability to the transport protein of Fe^{3+} kept in solution at neutral pH as the NTA complex is demonstrated in Fig. 4.

Reconstitution of the divalent metal ion transporter

The metal ion transport protein of the BBM can be solubilized and reconstituted into an artificial membrane system (Fig. 8). The same methodology was used before for the solubilization and reconstitution of other integral proteins of the BBM. Sucrase-isomaltase, the sodium-dependent glucose carrier (Kessi et al., 1994), and the scavenger receptor class B, type I (Hauser et al., 1998), were all reconstituted successfully in the same way as the divalent metal ion transport protein. From this analogy we conclude that the facilitated transport of divalent metal ions is due to an integral protein of the BBM. The equilibrium value of Fe^{2+} transport reconstituted into membrane vesicles and expressed as specific transport activity was increased by a factor of ~10 compared to the original BBMVs (Fig. 8). This is due to the fact that during the solubilization-reconstitution procedure cytoskeletal and cytosolic proteins are separated from the solubilized integral membrane proteins. This was shown to be the case for the solubilization and reconstitution of scavenger receptor class B, type I, of the BBM (Boffelli et al., 1997). The loss of proteins other than integral membrane proteins led to a significant increase in the specific activity of this receptor. Another possible explanation is that the volume of the vesicle cavity of the reconstituted vesicles is increased compared to the original BBMVs.

Temperature dependence of Ni^{2+} transport

Some important information on the divalent metal ion transport protein of the BBM can be derived from the temperature dependence of the pseudo-first-order rate constants (Fig. 3 *B*). The Arrhenius plot exhibits two break points, one at 5 ± 1°C and another one at 24 ± 1°C. Differential scanning calorimetry, electron spin resonance and fluorescence spectroscopy showed a broad gel-to-liquid crystal transition in both rat (Brasitus et al., 1980) and rabbit BBM (Mütsch et al., 1983). In the latter case this transition covers a temperature range from 10°C to 30°C (Hauser et al., 1982; Mütsch et al., 1983). The two break points in the Arrhenius plot are apparently related to the temperature range of the gel-to-liquid crystal transition: the lower break point occurs 5°C below the onset and the higher one 5°C below the completion temperature of the transition (Fig. 3 *B*). BBM-anchored enzymes such as sucrase-isomaltase and lactase have active centers that are located in the aqueous phase rather than within the lipid bilayer of the membrane. Consequently, Arrhenius plots of these enzymes were shown to have no break points (Brasitus et al., 1979; Mütsch et al., 1983). In contrast, membrane-spanning enzymes such as the Ca^{2+}/Mg^{2+}-dependent ATPase and the D-glucose transporter exhibit break points in the Arrhenius plot within the temperature range of the thermal lipid transition of the BBM (Brasitus et al., 1979; Mütsch et al., 1983). We interpret the breakpoints in the Arrhenius plot (Fig. 3 *B*) as evidence that the metal ion transporter of the BBM senses the gel-to-liquid crystal transition. We conclude that the divalent metal ion transporter is a membrane-spanning protein, very likely an ion channel. The value of the activation energy $E_a = 5.1$ kcal/mol derived from the straight-line portion of the Arrhenius plot above 5°C (Fig. 3 *B*) agrees within the error of the measurement with the activation energy reported for the Na^+-dependent D-glucose transporter in the rat BBMVs (Brasitus et al., 1979) but is about half of the value reported by Mütsch et al. (1983) for the same protein in rabbit BBM. The metal ion transport above the second break point is characterized by an activation energy of $E_a = 14.8$ kcal/mol. This is probably the value representative of metal ion transport by the divalent-metal ion transporter embedded in the liquid-crystalline bilayer of the BBM. The lower activation energy of $E_a = 5.1$ kcal/mol at temperatures below 24°C is representative of the BBM undergoing the crystal-to-liquid crystal phase transition and may reflect packing defects in the membrane present in this temperature range. Such defects could account for the difference in the E_a values below and above 24°C and for the fact that proton cotransport is only observed at temperatures equal to or greater than 24°C in the liquid-crystalline state of the membrane (Figs. 5, 6, and 8). Proton-coupled metal ion transport

observed under these conditions generates a proton gradient opposing the transport of further metal ions. This may at least partly account for the higher activation energy E_a = 14.8 kcal/mol observed under these conditions.

CONCLUSIONS

Recently a rat intestinal divalent-cation transporter, DCT1 or Nramp2, was identified by expression cloning in *Xenopus laevis* (Gunshin et al., 1997). It is a ubiquitous protein consisting of 561 amino acids with 12 putative membrane-spanning domains. The protein appears to be enriched in the duodenum, showing a distinct proximal-to-distal gradient of expression as detected by high-stringency Northern blotting. It has an unusually broad substrate specificity and mediates the transport of divalent cations such as Mn^{2+}, Fe^{2+}, Co^{2+}, Ni^{2+}, Cu^{2+}, Zn^{2+}, Cd^{2+}, and Pb^{2+}, which is driven by a proton-electrochemical gradient. There is a striking similarity in properties between DCT1 and the divalent-cation transporter described here. The two proteins share the broad substrate range, the substrate specificity, and the proton-coupled transport of divalent metal ions. Based on this correlation, we propose that the two proteins are either identical or at least closely related. We can conclude that a protein of the Nramp family, very likely Nramp2, occurs in the small-intestinal BBM, facilitating the transport of Fe^{2+} and other divalent transition metal ions. Most recently Canonne-Hergaux et al. (1999) provided immunoblot evidence showing that Nramp2 is indeed localized in the intestinal BBM of enterocytes and that this protein is absent from the basolateral membrane of these cells. While this paper was reviewed, a publication appeared by Tandy et al. (2000) showing that Nramp2 is also expressed in the apical plasma membrane of Caco-2 TC7 cells, but not in the basolateral part of the plasma membrane. Nramp2 was shown to be responsible for proton-coupled iron transport in these cells. Because the amino acid sequence of several members of the Nramp family is known (Gunshin et al., 1997), a promising approach would be to raise antibodies against the fourth extracellular (luminal) loop of Nramp2 and test the effect of these antibodies on divalent metal ion transport in BBM models.

We thank Mr. Alexander Tchouboukov and Ms. Barbara Schnüriger for their expert technical assistance.

This work was supported by Vifor (International) AG, the Swiss National Science Foundation (grants 31-49726.96 and 32-46810.96), and the Swiss Federal Institute of Technology, Zurich.

REFERENCES

Alvarez-Hernandez, X., M. Smith, and J. Glass. 1994. Regulation of iron uptake and transport by transferrin in Caco-2 cells, an intestinal cell line. *Biochim. Biophys. Acta.* 1192:215–222.

Boffelli, D., F. E. Weber, S. Compassi, M. Werder, G. Schulthess, and H. Hauser. 1997. Reconstitution and further characterization of the cholesterol transport activity of the small-intestinal brush border membrane. *Biochemistry.* 36:10784–10792.

Brasitus, T. A., D. Schachter, and T. G. Mamouneas. 1979. Functional interactions of lipids and proteins in rat intestinal microvillus membranes. *Biochemistry.* 18:4136–4144.

Brasitus, T. A., A. R. Tall, and D. Schachter. 1980. Thermotropic transitions in rat intestinal plasma membranes studied by differential scanning calorimetry and fluorescence polarization. *Biochemistry.* 19:1256–1261.

Breuer, W., S. Epsztejn, P. Millgram, and I. Z. Cabantchik. 1995. Transport of iron and other transition metals into cells as revealed by a fluorescent probe. *Am. J. Physiol.* 268:C1354–C1361.

Canonne-Hergaux, F., S. Gruenheid, P. Ponka, and P. Gros. 1999. Cellular and subcellular localization of the Nramp2 iron transporter in the intestinal brush border and regulation by dietary iron. *Blood.* 93:4406–4417.

Conrad, M. E., J. N. Umbreit, E. G. Moore, and D. Heiman. 1996. Mobilferrin is an intermediate in iron transport between transferrin and hemoglobin in K562 cells. *J. Clin. Invest.* 98:1449–1454.

Conrad, M. E., J. N. Umbreit, E. G. Moore, R. D. Peterson, and M. B. Jones. 1990. A newly identified iron binding protein in duodenal mucosa of rats. Purification and characterization of mobilferrin. *J. Biol. Chem.* 265:5273–5279.

Dautry-Varsat, A., A. Ciechanover, and H. F. Lodish. 1983. pH and the recycling of transferrin during receptor-mediated endocytosis. *Proc. Natl. Acad. Sci. USA.* 80:2258–2262.

De Silva, D. M., C. C. Askwith, and J. Kaplan. 1996. Molecular mechanisms of iron uptake in eukaryotes. *Physiol. Rev.* 76:31–47.

Fleming, M. D., M. A. Romano, M. A. Su, L. M. Garrick, M. D. Garrick, and N. C. Andrews. 1998. Nramp2 is mutated in the anemic Belgrade (b) rat: evidence of a role for Nramp2 in endosomal iron transport. *Proc. Natl. Acad. Sci. USA.* 5:1148–1153.

Fleming, M. D., C. C. Trenor, M. A. Su, D. Foernzler, D. R. Beier, W. F. Dietrich, and N. C. Andrews. 1997. Microcytic anaemia mice have a mutation in Nramp2, a candidate iron transporter gene. *Nature Genet.* 16:383–386.

Glahn, R. P., E. M. Wien, D. R. Van Campen, and D. D. Miller. 1996. Caco-2 cell iron uptake from meat and casein digests parallels in vivo studies: use of a novel in vitro method for rapid estimation of iron bioavailability. *J. Nutr.* 126:332–339.

Gruenheid, S., M. Cellier, S. Vidal, and P. Gros. 1995. Identification and characterization of a second mouse Nramp gene. *Genomics.* 25: 514–525.

Gunshin, H., B. Mackenzie, U. V. Berger, Y. Gunshin, M. F. Romero, W. F. Boron, S. Nussberger, J. L. Gollan, and M. A. Hediger. 1997. Cloning and characterization of a mammalian proton-coupled metal-ion transporter. *Nature.* 388:482–488.

Gutierrez, J. A., and M. Wessling-Resnick. 1996. Molecular mechanisms of iron transport. *Crit. Rev. Eukaryot. Gene Exp.* 6:1–14.

Gutierrez, J. A., J. Yu, and M. Wessling-Resnick. 1998. Characterization and chromosomal mapping of the human gene for SFT, a stimulator of Fe transport. *Biochem. Biophys. Res. Commun.* 253:739–742.

Haase, W., A. Schafer, H. Murer, and R. Kinne. 1978. Studies on the orientation of brush-border membrane vesicles. *Biochem. J.* 172:57–62.

Han, O., M. L. Failla, A. D. Hill, E. R. Morris, and J. C. Smith Jr. 1995. Reduction of Fe(III) is required for uptake of nonheme iron by Caco-2 cells. *J. Nutr.* 125:1291–1299.

Hauser, H., J. H. Dyer, A. Nandy, M. A. Vega, M. Werder, E. Bieliauskaite, F. E. Weber, S. Compassi, A. Gemperli, D. Boffelli, E. Wehrli, G. Schulthess, and M. C. Phillips. 1998. Identification of a receptor mediating absorption of dietary cholesterol in the intestine. *Biochemistry.* 37:17843–17850.

Hauser, H., N. Gains, and M. Mueller. 1983. Vesiculation of unsonicated phospholipid dispersions containing phosphatidic acid by pH adjustment: physicochemical properties of the resulting unilamellar vesicles. *Biochemistry.* 22:4775–4781.

Hauser, H., N. Gains, G. Semenza, and M. Spiess. 1982. Orientation and motion of spin-labels in rabbit small intestinal brush border vesicle membranes. *Biochemistry.* 21:5621–5628.

Hauser, H., K. Howell, R. M. Dawson, and D. E. Bowyer. 1980. Rabbit small intestinal brush border membrane preparation and lipid composition. *Biochim. Biophys. Acta.* 602:567–577.

Huebers, H. A., E. Huebers, E. Csiba, W. Rummel, and C. A. Finch. 1987. The cadmium effect on iron absorption. *Am. J. Clin. Nutr.* 45: 1007–1012.

Jordan, I., and J. Kaplan. 1994. The mammalian transferrin-independent iron transport system may involve a surface ferrireductase activity. *Biochem. J.* 302:875–879.

Kessi, J., J. C. Poiree, E. Wehrli, R. Bachofen, G. Semenza, and H. Hauser. 1994. Short-chain phosphatidylcholines as superior detergents in solubilizing membrane proteins and preserving biological activity. *Biochemistry.* 33:10825–10836.

Klip, A., S. Grinstein, and G. Semenza. 1979. Transmembrane disposition of the phlorizin binding protein of intestinal brush borders. *FEBS Lett.* 99:91–96.

Marx, J. J., and P. Aisen. 1981. Iron uptake by rabbit intestinal mucosal membrane vesicles. *Biochim. Biophys. Acta.* 649:297–304.

Mütsch, B., N. Gains, and H. Hauser. 1983. Order-disorder phase transition and lipid dynamics in rabbit small intestinal brush border membranes. Effect of proteins. *Biochemistry.* 22:6326–6333.

Perevucnik, G., P. Schurtenberger, D. D. Lasic, and H. Hauser. 1985. Size analysis of biological membrane vesicles by gel filtration, dynamic light scattering and electron microscopy. *Biochim. Biophys. Acta.* 821: 169–173.

Perewusnyk, G., and F. Funk. 1997. Iron uptake by rabbit brush border membrane vesicles involves movement through the outer surface, membrane interior, inner surface and aqueous interior. *J. Nutr.* 127: 1092–1098.

Qian, Z. M., P. L. Tang, and Q. Wang. 1997. Iron crosses the endosomal membrane by a carrier-mediated process. *Prog. Biophys. Mol. Biol.* 67:1–15.

Raja, K. B., R. J. Simpson, and T. J. Peters. 1992. Investigation of a role for reduction in ferric iron uptake by mouse duodenum. *Biochim. Biophys. Acta.* 1135:141–146 (erratum: 1176:197).

Savigni, D. L., and E. H. Morgan. 1998. Transport mechanisms for iron and other transition metals in rat and rabbit erythroid cells. *J. Physiol. (Lond.).* 508:837–850.

Schulthess, G., S. Compassi, D. Boffelli, M. Werder, F. E. Weber, and H. Hauser. 1996. A comparative study of sterol absorption in different small-intestinal brush border membrane models. *J. Lipid Res.* 37: 2405–2419.

Semenza, G., M. Kessler, M. Hosang, J. Weber, and U. Schmidt. 1984. Biochemistry of the Na^+, D-glucose cotransporter of the small-intestinal brush-border membrane. The state of the art in 1984. *Biochim. Biophys. Acta.* 779:343–379.

Smythe, E., and G. Warren. 1991. The mechanism of receptor-mediated endocytosis. *Eur. J. Biochem.* 202:689–699.

Tandy, S., M. Williams, A. Leggett, M. Lopez-Jimenez, M. Dedes, B. Ramesh, S. K. Srai, and P. Sharp. 2000. Nramp2 expression is associated with pH-dependent iron uptake across the apical membrane of human intestinal Caco-2 cells. *J. Biol. Chem.* 275:1023–1029.

Thurnhofer, H., and H. Hauser. 1990. The uptake of phosphatidylcholine by small intestinal brush border membrane is protein-mediated. *Biochim. Biophys. Acta.* 1024:249–262.

Trowbridge, I. S. 1991. Endocytosis and signals for internalization. *Curr. Opin. Cell Biol.* 3:634–641.

Umbreit, J. N., M. E. Conrad, E. G. Moore, and L. F. Latour. 1998. Iron absorption and cellular transport: the mobilferrin/paraferritin paradigm. *Semin. Hematol.* 35:13–26.

Vidal, S. M., D. Malo, K. Vogan, E. Skamene, and P. Gros. 1993. Natural resistance to infection with intracellular parasites: isolation of a candidate for Bcg. *Cell.* 73:469–485.

Wienk, K. J., J. J. Marx, A. G. Lemmens, E. J. Brink, R. Van Der Meer, and A. C. Beynen. 1996. Mechanism underlying the inhibitory effect of high calcium carbonate intake on iron bioavailability from ferrous sulphate in anaemic rats. *Br. J. Nutr.* 75:109–120.